Available online at www.sciencedirect.com
SCIENCE DIRECT®
Bioelectrochemistry 61 (2003) 73–84
Bioelectrochemistry
www.elsevier.com/locate/bioelechem

Energetics and mechanisms of high efficiency of charge separation and electron transfer processes in *Rhodobacter sphaeroides* reaction centers

Vladimir Z. Paschenko[a,*], Vladimir V. Gorokhov[a], Peter P. Knox[a], Pavel M. Krasilnikov[a], Harald Redlin[b], Gernot Renger[c], Andrew B. Rubin[a]

[a] *Department of Biophysics, Biology Faculty, Lomonosov State University, Moscow 119899, Russia*
[b] *Max-Born-Institute, Berlin D-12489, Germany*
[c] *Max-Volmer-Institute, Technical University, Berlin D-10623, Germany*

Received 18 January 2003; received in revised form 7 June 2003; accepted 19 June 2003

Abstract

Effects of environmental changes due to D_2O/H_2O substitution and cryosolvent addition on the energetics of the special pair and the rate constants of forward and back electron transfer reactions in the picosecond–nanosecond time domain have been studied in isolated reaction centers (RC) of the anaxogenic purple bacterium *Rhodobacter sphaeroides*. The following results were obtained: (i) replacement of H_2O by D_2O or addition of either 70% (v/v) glycerol or 35% (v/v) DMSO do not influence the absorption spectra; (ii) in marked contrast to this invariance of absorption, the maxima of fluorescence spectra are red shifted relative to control by 3.5, 6.8 and 14.5 nm for RCs suspended in glycerol, D_2O or DMSO, respectively; (iii) D_2O/H_2O substitution or DMSO addition give rise to an increase of the time constants of charge separation (τ_e), and Q_A^- formation (τ_Q) by a factors of 2.5–3.1 and 1.7–2.5, respectively; (iv) addition of 70% glycerol is virtually without effect on the values of τ_e and τ_Q; (v) the midpoint potential E_m of P/P^+ is shifted by about 30 and 45 mV towards higher values by addition of 70% glycerol and 35% DMSO, respectively, but remains invariant to D_2O/H_2O exchange; and (vi) an additional fast component with $\tau_1 = 0.5–0.8$ ns in the kinetics of charge recombination $P^+H_A^- \rightarrow P^*(P)H_A$ emerges in RC suspensions modified either by D_2O/H_2O substitution or by DMSO treatment.

The results have been analysed with special emphasis on the role of deformations of hydrogen bonds for the solvation mechanism of nonequilibrium states of cofactors. Reorientation of hydrogen bonds provides the major contribution of the very fast environmental response to excitation of the special pair P. The Gibbs standard free energy gap between $^1P^*$ and $P^+B_A^-$ due to solvation is estimated to be ~ 70, 59 and 48 meV for control, D_2O- and DMSO-treated RC samples, respectively.

Keywords: Reaction center; Hydrogen bond; Nonequilibrium cofactor state; Relaxation process; Electron transfer

1. Introduction

The transformation of solar radiation into electrochemical free energy takes place in specialized membrane bound pigment–protein complexes referred to as reaction centers (RC). One of the most thoroughly analyzed systems among the photosynthetic organisms is the RC of the purple bacterium *Rhodobacter (Rb.) sphaeroides*. For this system, the crystal structure is known at high resolution and the rate constants of the individual electron transfer steps of the photoinduced charge separation are well characterized (for reviews, see Refs. [1,2]). The RC is consisting of three polypeptides (subunits L, M and H) and contains four bacteriochlorophyll-a (BChl-a), two bacteriopheophytin-a (BPheo-a) and two ubiquinone (Q_A and Q_B) molecules, one carotenoid species and a non-heme iron center. Two of the four BChl-a molecules form a strongly coupled special pair (P) that serves as electron donor for the light-induced

Abbreviations: BChl, bacteriochlorophyll; BPheo, bacteriopheophytin; RC, reaction center; P or P_BP_A, primary electron donor; B_A, primary electron acceptor $BChl_A$; H_A, electron acceptor $Bpheo_A$; Q_A, primary quinone; DMSO, dimethylsulphoxide; $^1P_i^*B_AH_AQ_A$, initial excited state of RC; $^1P_r^*B_AH_AQ_A$, relaxed excited state of RC.

* Corresponding author. Fax: +7-95-939-1115.
E-mail address: paschenko@biophys.msu.ru (V.Z. Paschenko).

1567-5394/$ - see front matter © 2003 Elsevier B.V. All rights reserved.
doi:10.1016/S1567-5394(03)00077-X

reaction sequence. All pigments are bound to the heterodimeric protein matrix of subunits L and M each forming five transmembrane helices with pseudo-C_2 symmetry. This structure gives rise to cofactor binding in two branches referred to as A and B sides of RC [1,3–5]. Despite this apparently symmetrical structural arrangement, the light-induced vectorial electron transfer from $^1P^*$ to Q_A in RCs from WT purple bacteria comprises only the chromophores on the A side including the monomeric BChl-a (B_A) and BPheo-a (H_A) as intermediate redox carriers [1–5]. A change of this functional unidirectionality can be only achieved by replacement of key amino residues via genetic engineering that also changes the cofactor composition [6–9]. Recently, a yield of 35–45% was reported for the $P^+H_B^-$ formation in the inactive B-branch of a quadruple mutant of *Rb. sphaeroides*. However, further electron transfer from H_B^- to ubiquinone was negligibly (<1%) small [7]. In the *Rb. capsulata* YFHV mutant, the electron transfer to the B-side bacteriopheophytin H_B and further to quinone acceptor Q_B leads to formation of $P^+H_B^-$ and $P^+Q_B^-$ with a yield of 30% and 10–25%, respectively [8]. Likewise, in *Rb. sphaeroides*, mutants where Q_A binding is prevented by mutation of Ala M260 to Trp, light-induced charge separation via the B branch is established and $P^+Q_B^-$ formed with yields up to 50% in quadruple mutants [9].

After formation of the electronically excited singlet-state $^1P^*$ a rapid (~ 3.5 ps) charge separation takes place. It is now well established that the electron transfer steps along the active A-branch follow a sequential mechanism where the anion radicals of monomeric BChl-a (B_A^-), BPheo-a (H_A^-) and ubiquinone (Q_A^-) are formed with time constants of 3, 0.9 and 200 ps, respectively [10–13]. The electron transfer reactions are coupled with the vibrational dynamics of cofactors and the surrounding protein matrix. The possible role of specific vibrations for the electron transfer has been illustrated in a recent study that is based on quantum chemical calculations of the pigment molecules in *Rb. sphaeroides* RC. The results obtained led to the conclusion that torsional modes of the acetyl group of ring I of the BChl moieties in special pair P [14] as well as the axial coordination of His to P [15] are likely to be involved in charge separation processes. Besides that, hydrogen bonds between H_A and amino acid residues lower the LUMO energy of H_A and incite the electron transfer along A-branch in the wild-type RC of *Rb. sphaeroides* [15].

In addition to these specific modes, microconformational alterations of the media accompany electron transfer reactions that regulate via kinetic modulations the efficiency of the charge separation. The conformational dynamics can promote specific structural configurations around the redox active cofactors, so that the forward electron transfer becomes strongly favored compared with the corresponding back reactions. Experimental evidence for the stabilization of the radical ion pair $P^{+\cdot}H_A^{-\cdot}$ by protein relaxation has been recently gathered from photovoltage measurements in chromatophores of *Rhodospirillum rubrum* [16]. Furthermore, evidence has been presented for the existence of long living radical pairs $P^{+\cdot}Q_A^{-\cdot}$ owing to significant conformational changes of the protein structure [17]. However, the details of the steerage via protein dynamics are still not clarified.

The mode of cofactor interaction with both, the protein matrix itself and its water–protein surrounding can be modified by various means. Essentially, two different techniques can be used: (i) replacement of individual amino acids by site-directed mutagenesis or (ii) alteration of the dielectric environment, especially of H-bond networks, either through D_2O/H_2O exchange or by addition of suitable solvent molecules (e.g. DMSO).

Using the first approach, a series of mutants have been constructed where especially the hydrogen bonding of the special pair P were modified [18–23]. It was shown that deletion of the single hydrogen bond to the carbonyl group of BChl-a in P of the wild type causes a decrease of the midpoint potential of P by about 85 mV, while insertion of additional hydrogen bonding leads to an incremental increase by about 85 mV per bond [22,23]. Likewise, the rate constant of $P^+H_A^-$ formation decreases from 3.5 to 40 ps^{-1}. On the other hand, removal of the hydrogen bond to the keto carbonyl group of BPheo by replacing Glu 104 of the L-subunit is of marginal effect on the kinetics of charge separation to $P^+Q_A^-$ [24].

By using the second approach, i.e. replacement of exchangeable protons by deuterons and/or by adding cryosolvents, we were able to show that the rate constants of both, $P^+H_A^-$ formation and subsequent electron transfer from H_A^- to Q_A can be changed by a factor of 2–3 [25–28].

The present paper describes further experimental data obtained with RCs in suspensions containing either cryoprotectants or D_2O. Furthermore, based on theoretical calculations, the modification of hydrogen bonds and effects on the energetics and kinetics of charge separation caused either by H/D exchange or addition of DMSO or glycerol are analyzed within the framework of simplified models.

2. Materials and methods

RC preparations were isolated from chromatophores of wild type *Rb. sphaeroides*. After incubation of chromatophores for 30 min at 4 °C in a reaction medium containing 10 mM sodium–phosphate buffer (pH 7.0) and 0.5% LDAO and centrifugation for 2 h at 144 000 × *g*, the RC preparation was separated chromatographically on an oxyapatite column as described in [29].

Redox titrations were performed with RCs suspended in 50 mM Tris–HCl buffer (pH 7.5) containing 0.05% LDAO. For measurements of flash-induced absorption changes in the picosecond time domain by using a pump-and-probe method, the RCs were suspended in 10 mM Tris–HCl buffer (pH 8.0) containing 0.025% sodium cholate. This medium was found to be most appropriate to minimize denaturation caused by drying and subsequent resuspension in H_2O (D_2O)

and prevent aggregation at high sample concentrations (P870 concentration of about 0.5 mM) that are necessary for measurements at high time resolution.

For replacement of H_2O by D_2O, RC preparations were lyophilized for 2.5–3 h at a pressure of 13 Pa and resuspended in D_2O (isotopic substitution efficiency, 99.8%) or in H_2O (control).

Glycerol was added to the samples at a concentration of up to 70 vol.%. A similar addition is widely used for optical measurements at low temperatures because it favors the formation of suitable glasses. DMSO was added to a concentration of 35% (v/v) in accordance with the data in Ref. [25] on the DMSO effect on the functional activity of RC.

Absorption spectra were recorded with of a spectrometer Hitachi 557. Fluorescence spectra were measured with a spectrophotometer SPEX Fluorolog. Inside the spectrophotometer the photocathode was cooled down to −70 °C during measurements.

The time course of the absorption changes reported in former studies [26–28] were numerically reanalysed on the basis of a set of coupled differential equations describing the transitions in the RC and using a fit by varying its parameters (target analysis). The numerical solution of the set of coupled differential equations was convoluted with a function $\varphi(t)$ simulating the shape of the probing laser pulse ($\varphi(t)$ as Gaussians with a half-width of 5 ps).

3. Results

3.1. Spectral properties

Figs. 1 and 2 depict steady-state absorption and fluorescence spectra, respectively, of RCs isolated from *Rb. sphaeroides* and suspended in standard buffer or modified either by using D_2O instead of H_2O or by addition of DMSO or glycerol. The data of Fig. 1 reveal that the absorption spectra are virtually identical for all types of samples. Therefore, it can be concluded that neither replacement of exchangeable protons by deuterons nor addition of glycerol or DMSO leads to modifications of the protein matrix that give rise to changes of the interaction between the environment and the pigments P, BCl and BPheo in their ground state.

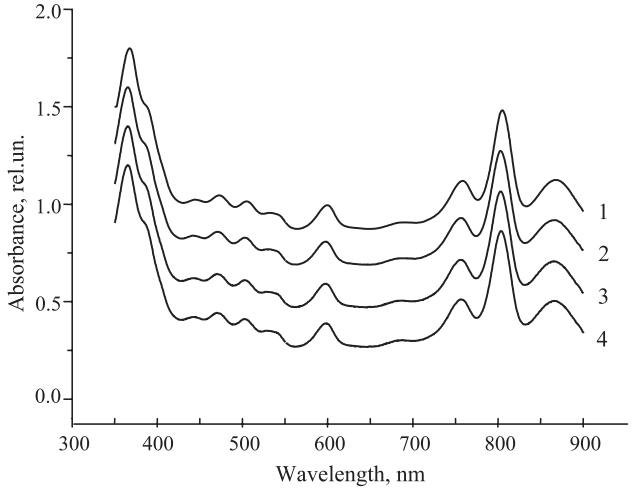

Fig. 1. Absorption spectra of the *Rb. sphaeroides* RC preparations used for investigation. (1) Control samples, (2) addition of 70% (v/v) glycerol, (3) RC modified by D_2O/H_2O substitution and (4) samples modified by DMSO 35% (v/v).

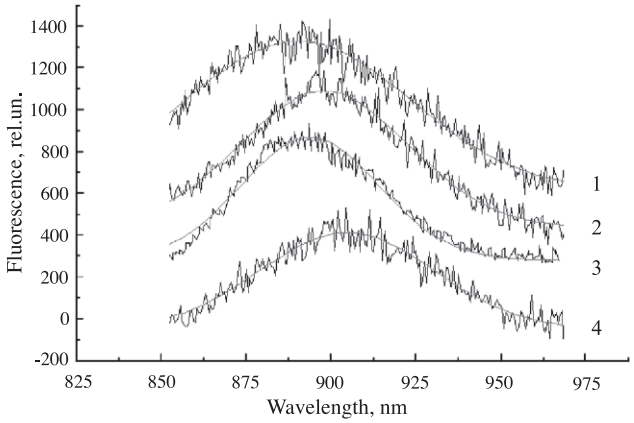

Fig. 2. Fluorescence spectra of the RC *Rb. sphaeroides* RC preparations. (1) Control samples, (2) RC modified by D_2O/H_2O substitution, (3) addition of 70% (v/v) glycerol and (4) samples modified by DMSO 35% (v/v) addition.

The fluorescence spectra were measured at an actinic wavelength of 800 nm where the monomeric BCl molecules are excited. The quantum yield of energy transfer from BCl to P870 was reported to be 93% [30]. The optical density of the samples at 800 nm was small (0.07–0.08) in order to assure that self-absorption of the fluorescence was insignificant.

An inspection of the data readily shows that, in marked contrast to the absorption properties (see Fig. 1), the fluorescence emission is significantly affected by the type of RCs suspension medium. For quantitative evaluation, the experimental fluorescence spectra were fitted by a Gaussian function:

$$I(\lambda) = I_{\max}\exp\left(-\frac{4(\lambda-\lambda_{\max})^2}{(\Delta\lambda_{1/2})^2}\ln 2\right) \quad (1)$$

where $I_{\max}$ is the emission at the maximum of the band, $\lambda_{\max}$ is the wavelength of the fluorescence band maximum and $\Delta\lambda_{1/2}$ is the FWHM of the fluorescence spectrum. The relative fluorescence quantum yield in differently modified samples, ϕ, normalized to that of the untreated control, ϕ_0, was calculated according to the relation [31]:

$$\phi/\phi_0 = (S/S_0)(\beta/\beta_0)(n^2/n_0^2) \quad (2)$$

where S, S_0 are the areas of the fluorescence spectra; β, β_0 the fractions of the light absorbed and n, n_0 the refractive indices of modified and control samples, respectively. The value of β/β_0 is obtained from the relation $(1-10^{-A})/(1-$

10^{-A_0}), where A and A_0 is the optical density of modified sample and control, respectively, at excitation wavelength $\lambda_{ex} = 800$ nm.

Table 1 compiles the values of λ_{max}, $\Delta\lambda_{1/2}$ and $\varphi = \phi/\phi_0$ gathered from a numerical fit of the experimental data by Eqs. (1) and (2). These data reveal that the maxima of the fluorescence spectra are red shifted relative to the control by 3.5, 6.8 and 14.5 nm for RCs suspended in buffer containing glycerol, D_2O or DMSO, respectively. The shifts correspond with a decrease in energy, ΔE, with values that are presented in the second column of Table 1. These slight energy downshifts are ascribed to modified fast relaxation processes of the protein matrix that take place during the lifetime of the excited singlet states in the Q_y region.

The changes of λ_{max} are accompanied by a decrease of the FWHM values of the modified RC. This band narrowing of the fluorescence spectra after replacement of exchangeable protons or addition of glycerol or DMSO is explainable by an increase of the rigidity of the protein matrix, in line with conclusions reported previously by Luck and Kleeberg for the cryosolvents [32,33]. Furthermore, Table 1 also shows that the relative fluorescence quantum yield of the RC preparation is raised by a factor 1.8 for glycerol-treated RC and decreased by a factor 0.65 for RC suspended in DMSO. In our opinion, this fact originates from differences in the effects of glycerol and DMSO on the protein structure (see below).

3.2. Modification of the rate constants k_e and k_Q of light-induced charge separation and electron transfer to Q_A

The photoinduced electron transfer sequence in RCs of *Rb. sphaeroides* can be described by a simple scheme:

$$PB_AH_AQ_A \xrightarrow{h\nu} P^*B_AH_AQ_A \xrightarrow{\tau_e=3.5\ ps} P^+B_AH_A^-QA \xrightarrow{\tau_Q=200\ ps} P^+B_AH_AQ_A^- \quad (3)$$

Our experimental data related to the τ_e and τ_Q measurement previously published in Refs. [26–28] are reanalysed numerically and the results obtained shown in Fig. 6 for control, D_2O/H_2O substitution and DMSO-treated RCs. For better illustration, the data reported in Refs. [26–28] for τ_e and τ_Q in control and modified suspensions of RCs are compiled in Table 2. It shows that D_2O/H_2O substitution and DMSO addition give rise to a 2.5–3.1-fold increase in τ_e, whereas the τ_Q value is raised by a factor of 1.7–2.5. On the other hand, addition of 70% glycerol does virtually not affect the τ_e and τ_Q values.

Table 1
Parameters of the fluorescence spectra depicted in Fig. 2, calculated according to relations (1) and (2)

Sample	λ_{max}, nm	ΔE, meV	$\Delta\lambda_{1/2}$, nm	φ
Control	890.2	–	77.7	1.0
75% glycerol	893.7	5.5	47.8	1.80
D_2O/H_2O exchange	897.0	10.7	58.5	0.96
35% DMSO	904.7	22	61	0.65

λ_{max} represents the wavelength position of the maximum in the fluorescence spectrum; ΔE is the energetic shift of the fluorescence maximum relative to the control sample; $\Delta\lambda_{1/2}$ is the FWHM of the spectrum; φ is the relative fluorescence quantum yield.

Table 2
Reaction times τ_e and τ_Q for $P^+H_A^-$ formation and electron transfer from H_A^- to Q_A, respectively, and midpoint potentials E_m of the primary electron donor P of RCs from *Rb. sphaeroides*

Parameters	Control	$H_2O \rightarrow D_2O$ exchange	70% glycerol addition	35% DMSO addition
$\tau_{e,\ ps}$	3.4 ± 0.5	8.5 ± 0.5	3.5 ± 0.5	10.8 ± 0.8
$\tau_{Q,\ ps}$	205 ± 5	350 ± 10	230 ± 5	510 ± 20
E_m, mV	430	430	460	475

In the experiments, RC preparations were used suspended in control buffer or modified by H_2O/D_2O exchange or addition of either glycerol (70% v/v) or DMSO (35% v/v).

For a comparison of kinetic and energetic effects, the last row of Table 2 presents our results of redox titrations of P/P^+ in these samples [27,34]. An inspection of Table 2 shows that no direct correlation exists between a shift of E_m and changes of rate constants $k_e = 1/\tau_e$ and $k_Q = 1/\tau_Q$ of the two electron transfer steps. Addition of 70% (v/v) glycerol shifts the P/P^+ potential by 30 mV but is virtually without effect on τ_e and τ_Q. An opposite phenomenon emerges when all exchangeable protons are replaced by deuterons. In this case, the kinetics of the electron transfer steps are markedly retarded ($\tau_e \cong 8.5$ ps and $\tau_Q \cong 350$ ps), while E_m remains unaffected. On the other hand, in the presence of 35% (v/v) DMSO instead of glycerol both, energetics (upshift of E_m by 45 mV) and kinetics ($\tau_e \cong 10.8$ ps and $\tau_Q \cong 510$ ps) are affected.

3.3. Charge recombination $P^+B_AH_A^- \rightarrow P^*(P)B_AH_A$

If the electron transfer from H_A^- to Q_A is blocked ($k_Q = 0$, Eq. (3)) either keeping Q_A^- reduced or by extraction of Q_A, the lifetime of the ion-radical pair $P^+H_A^-$ raises from about 200 ps (reoxidation of H_A^- by Q_A) in the untreated control samples up to 11–13 ns [26,35,36]. In this case, the recombination between P^+ and H_A^- dominates the overall reaction. It was found [26] that the kinetics of laser flash-induced absorption changes $\Delta A(t)$ due to the transient decay of $P^+H_A^-$ in RCs with quinone Q_A chemically reduced in the dark could be fitted by:

$$\Delta A(t) = A_1\exp(-t/\tau_1) + A_2\exp(-t/\tau_2) + A_3 \quad (4)$$

where A_i, τ_i are the amplitudes and lifetimes of the fast, (A_1, τ_1) and slow (A_2, τ_2) component, A_3 reflects the efficiency of the triplet state (^3P) formation.

It was shown [26] that, within the accuracy of measurements (0.3% optical density changes) in control samples, the kinetics of the absorption changes at 665 nm reflecting the charge recombination between P^+ and H_A^- are monoexponential with $\tau_2 = 11.2$ ns, whereas the relaxation of ΔA870 as indicator of P^+ reduction exhibits a residual bleaching that persists for times $\gg 10$ ns with an amplitude $A_3 = 0.15$.

Table 3
Values of A_1, τ_1 and A_2,τ_2 gathered from a fit by Eq. (4) of the flash induced absorption changes ΔA665 of RCs from *Rb. sphaeroides* with Q_A^- kept chemically reduced in normal (control), D_2O or DMSO containing suspensions

Sample	A_1	τ_1, ns	A_2	τ_2, ns
Control	–	–	1.0	11.2
$H_2O \rightarrow D_2O$ exchange	0.35	0.5	0.65	11.0
35% DMSO addition	0.52	0.8	0.48	10.8

This value of A_3 corresponds to the portion of $P^+H_A^-$ pairs, which populate the triplet-state ^3P. A fast component τ_1 is not detected.

In marked contrast, however, in suspensions modified either by D_2O/H_2O substitution or by DMSO addition, the kinetics of DA665 and DA870 absorption changes exhibit an additional fast component with $\tau_1 = 0.5–0.8$ ns, while τ_2 remains virtually the same as in the control (see Table 3). These findings show that modification of hydrogen bond networks in RCs not only affects the electron transfer steps of the forward reactions but also significantly change the kinetic pattern of the recombination reaction between P^+ and H_A^-.

4. Discussion

The vast majority of biological redox processes are nonadiabatic reactions (for review, see Refs. [37,38] and references therein). In the absence of triggering by proton transfer or conformational changes, the rate constant k_{ET} of an electron transfer step is characterized by Eq. (5):

$$k_{ET} = \frac{2\pi}{\hbar} |V_{ET}|^2 (4\pi\lambda k_B T)^{-\frac{1}{2}} \exp\left[-\frac{(\Delta G^0 + \lambda)^2}{4\lambda k_B T}\right] \quad (5)$$

where V_{ET} is the quantum mechanical matrix element coupling initial and final electronic wavefunction, ΔG^0 the standard driving force (Gibbs free energy gap), λ the reorganization energy, T the temperature and k_B the Boltzman constant. Accordingly, k_{ET} can be regulated via modifications of $|V_{ET}|^2$, ΔG^0 or λ.

In the following description, effects of modifications induced either by suspending the RCs in D_2O or by addition of DMSO (glycerol) on the energetics and kinetics of electron transfer steps will be analyzed.

4.1. Effect of glycerol and DMSO on the midpoint potential E_m of P

The influence of a modifying treatment on the E_m value of the primary donor was analyzed earlier in details [27,39] using the Lorentz local field theory [40]. It was shown [27,39] that addition of glycerol and DMSO can change the macroscopic dielectric parameters and disturb the microscopic structure of the immediate surroundings of a redox group. The change of the midpoint potential E_m may be due to: (a) alteration of the dielectric constant of the surrounding, (b) swelling of the protein globule owing to penetration of solvent molecules and c) change in the positions of elementary charges within the nearest water–protein interior.

The considerations [27,39] reveal that the shift of the redox potential of P/P^+ observed in our experiments after the addition of cryoprotecting solvents (DMSO in particular) is predominantly caused by microscopic shifts of the charge positions in the vicinity of P.

It has to be emphasized that the considerations about cryoprotectant-induced effects on the midpoint potential presented earlier [27,39] and outlined in the present study do not assume a special character of the redox center in the RC structure. That means that DMSO and glycerol addition would upshift the midpoint potential of all cofactors by the same value. Hence, the mutual differences between the redox potentials of P/P^+, B_A^-/B_A, H_A^-/H_A and Q_A^-/Q_A and as a consequence also the rate constants of the electron transfer are expected to remain virtually invariant to the addition of cryoprotectants. This conclusion is in the line with the experimental findings for suspensions containing 70% glycerol but not for addition of DMSO (see Table 2). On the other hand, a marked retardation of the electron transfer reactions without detectable E_m shift is observed after replacement of exchangeable protons by deuterons. Obviously, in these cases the retardation of the electron transfer in modified RC *Rb. sphaeroides* is caused by other factors than the shift of P/P^+ midpoint potential.

4.2. Deformation of hydrogen bonds as a solvation mechanism of nonequilibrium states of cofactors

The kinetic effects caused by H/D exchange and addition of DMSO are assumed to originate from modified relaxation processes within hydrogen bond networks (in the case of DMSO one RC can bind an amount that almost corresponds with its own weight [41]). The addition of DMSO to H-bonded liquids causes an increase in the rigidity of their hydrogen bonds [32,33]. It is widely believed that there exists a relationship between the protein oscillations in the vicinity of cofactors and oscillations of the pigments themselves [42]. Protons of the water–protein environment are thought to be the primary intermediate of the interaction between nonequilibrium states of cofactors and the surrounding medium.

For further considerations, the energy spent for hydrogen bond deformation will be estimated. This process is assumed to be induced by the electric field $\vec{E}(\vec{r})$ of a central point charge $\pm e$ or a central dipole $\vec{p_0}$. A hydrogen bond in the protein molecule can be formed by water molecules and/or polar peptide groups that are in direct contact with each other. For the sake of simplicity, a model system is used where one hydrogen atom is located between two oxygen atoms ($O^-H\cdots O$). The restriction to oxygen atoms does not affect the general conclusions (analogous expressions are obtained for other atoms of biological relevance, like nitrogen). An electric dipole field $\vec{E}(\vec{r})$ acting on the proton

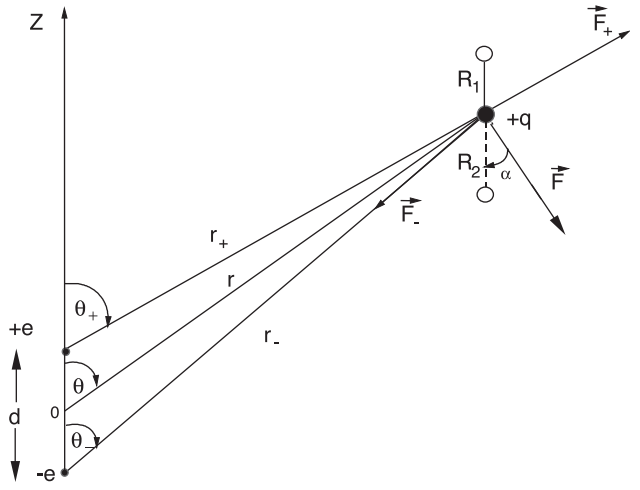

Fig. 3. Schematic diagram of forces applied to a positive charge q (proton) located between two negatively charged oxygen atoms. R_1 an R_2 are the distances between the proton and the oxygen atoms; d is the dipole base; r is the distance from the proton to the dipole; F is the equivalent force of the electrical field acting on the proton.

charge q causes its displacement from the initial equilibrium position, thereby inducing a deformation of the hydrogen bond. For a simplification of the calculation of the interaction energy between the force center and charge q, the far field approximation for the electric dipole field (Eq. (6)) is used, i.e. the distance between a dipole $p_0 = ed$ located at the origin of a polar coordinate system (Fig. 3) and the hydrogen bond is assumed to be large compared to the inner dipole distance d. Although this assumption is not justified for hydrogen bonds closest to a cofactor, the use of the far field approximation will still give the correct order of the interaction energy.

$$\vec{F} = q\vec{E}_{\text{dipole}} = \frac{q}{\varepsilon}\left(\frac{(\vec{p_0}\,\vec{r})\vec{r}}{r^5} - \frac{\vec{p_0}}{r^3}\right) \tag{6}$$

In general, the hydrogen-bond deformation induced by force $\vec{F}$ is the sum of longitudinal and transverse displacements of the proton relative to the line connecting the oxygen atoms. The energy of hydrogen-bond deformation was calculated assuming that the distance r between the force center and the proton is 4 Å (the distance from the tetrapyrrole ring of P_B and P_A to the key amino acid residues: histidine L168, L173 and M202; leucine L131 and M160 and phenylalanine L197).

In the case of longitudinal deformation (Fig. 4a), the proton displacement Δl can be calculated from the condition that the elastic and electric force are of equal size:

$$\Delta l = \frac{F_L}{k} = \frac{F\cos\alpha}{k} = \begin{cases} \dfrac{eq\cos\alpha}{k\varepsilon r^2} & \text{(central charge)} \\ \dfrac{p_0 q\cos\alpha}{k\varepsilon r^3}\sqrt{2\cos^2\theta+1} & \text{(central dipole)} \end{cases} \tag{7}$$

Here $k = k_1 + k_2$ where k_1 is the rigidity of the covalent bond O–H and k_2 is the rigidity of the hydrogen bond O· · ·H, θ the angle between dipole direction and the line connecting dipole and proton, α the angle between the line connecting the hydrogen and oxygen atoms and the vector of the force $\vec{F}$ (see Fig. 3) and ε the mean dielectric constant of the protein medium. The energy change owing to a longitudinal proton displacement can be calculated as $\Delta W_l = 1/2k(\Delta l)^2$. With the value for Δl taken from Eq. (7), one obtains:

$$\begin{aligned} \Delta W_l^{\text{e}} &= \frac{e^2q^2\cos^2\alpha}{2k\varepsilon^2r^4} && \text{(central charge)} \\ \Delta W_l^{\text{p}} &= \frac{p_0^2q^2(2\cos^2\theta+1)\cos^2\alpha}{2k\varepsilon^2r^6} && \text{(central dipole)} \end{aligned} \tag{8}$$

In the case of transverse deformation (Fig. 4b), the calculation yields a simplified expression for the energy $W_t^{\text{e,p}} = \frac{kR^2}{4}\left(\frac{F_T}{kR}\right)^{\frac{4}{3}}$ required for a transverse proton displacement:

$$\begin{aligned} \Delta W_t^{\text{e}} &= \frac{kR^2}{4}\left(\frac{eq\sin\alpha}{\varepsilon r^2 kR}\right)^{4/3} && \text{(central charge)} \\ \Delta W_t^{\text{p}} &= \frac{kR^2}{4}\left(\frac{p_0 q}{\varepsilon r^3 kR}\sqrt{(2\cos^2\theta+1)}\sin\alpha\right)^{4/3} && \text{(central dipole)} \end{aligned} \tag{9}$$

For further evaluation, we used the approximation $R = R_1 = R_2$; $k = k_1 = k_2$. To estimate the order of magnitude for $\Delta W_{l,t}^{\text{e}}$ and $\Delta W_{l,t}^{\text{p}}$ the following values for the parameters were used: $p_0 = 3D$; $q = 0.3e$; $\sin^2\alpha = \cos^2\alpha = \cos^2\theta = 1/2$; $r = 4$ Å; $R = 1$ Å; $k = 5\cdot10^4$ dyn/cm. As a result, the energy change due

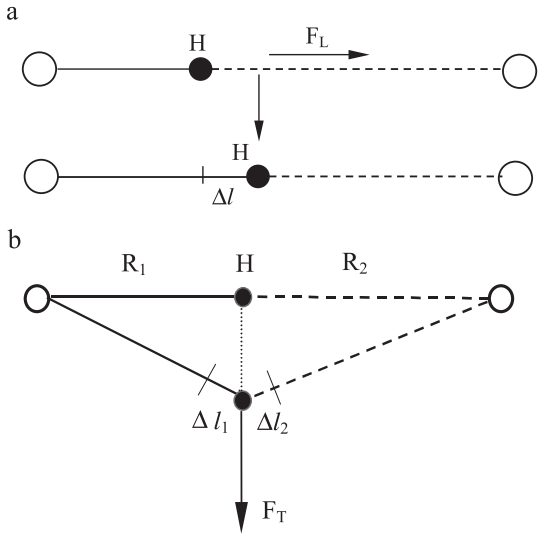

Fig. 4. Fundamental configurations describing the displacement of the proton induced by a central electric field: (a) longitudinal deformation of the hydrogen bond accompanied by elongation of the H-bond by the value of Δl; F_L is a longitudinal component of an electric force F; (b) transverse displacement of the proton with simultaneous elongation of the two bonds by the values of Δl_1 and Δl_2; R_1 and R_2 are the distances from the proton H to the oxygen atoms; F_T is a transverse component of an electric force F.

to deformation of one hydrogen bond is $\Delta W_l^e = 1.5 \cdot 10^{-3}$ eV, $\Delta W_l^p = 10^{-4}$ eV and $\Delta W_t^e \approx \Delta W_t^p \approx (3-5) \cdot 10^{-3}$ eV.

Thus, the average deformation energy of one hydrogen bond in the field of a central point charge or a central dipole can reach values of $5 \cdot 10^{-3}$ eV. Taking into account the number of hydrogen bonds in the vicinity of P (this number can be estimated from X-ray diffraction data [4,43]), the total energy decrease may reach values of 0.05 eV. This energy originates from solvation of the nonequilibrium state $^1P^*$ (or $(P_B^+P_A^-)$ and can be regarded as the medium reorganization energy λ (see Eq. (5)).

It should be pointed out that hydrogen bond deformation is the initial medium response owing to charge formation at the cofactor. Microconformational reorganization proceeds on a much longer time scale, gradually including larger structures, containing groups of atoms or fragments of a protein molecule. In general, the protein dynamics cover wide domains in time (10^{-15} up to 10^3 s) and space (local, large scale or collective) and are the most relevant modulators of the kinetics and energetics of electron transfer processes (for a review, see Refs. [44,45]).

4.3. Analysis of charge separation processes

Within the time scale of charge separation in bacterial RCs, only hydrogen bond deformation contributes to energy changes thus leading to transformation of the initially formed state $^1P_i^*$ into a "relaxed" state $^1P_r^*$. Thereby, the electronic level $^1P_i^*$ is lowered by about 0.05 eV. It appears likely that $^1P_r^*$ is the donator species for the sequential electron transfer to H_A via B_A. Taking into account the above considerations, the scheme of charge separation in bacterial RCs (Eq. (3)) can be written in the following form:

$$PB_AH_AQ_A \xrightarrow{h\nu} {}^1P_i^*B_AH_AQ_A \xrightarrow{k_r} {}^1P_r^*B_AH_AQ_A$$

$$\underset{(k_e')^-}{\overset{k_e'}{\rightleftarrows}} P^+B_A^-H_AQ_A \underset{(k_e'')^-}{\overset{k_e''}{\rightleftarrows}} P^+B_AH_A^-Q_A \xrightarrow{k_Q} P^+B_AH_AQ_A^- \tag{10}$$

Here $^1P_i^*$ and $^1P_r^*$ are the initial and relaxed (at the time scale of primary charge separation) states of the special pair, respectively; k_r the relaxation rate constant; k_e' the rate constant of charge separation; k_e'' the rate constant of electron transfer to H_A; and the other symbols are the same as in Eq. (3).

In former studies [46], a value of -0.07 ± 0.01 eV was reported for the free energy gap of the primary charge separation, i.e. ΔG_{12} between states $^1P^*B_AH_AQ_A$ and $P^+B_A^-H_AQ_A$ (see Fig. 5). For this determination, the energy of state $^1P^*B_AH_AQ_A$ was gathered [46] from the fluorescence spectrum and therefore represents the relaxed state $^1P_r^*B_AH_AQ_A$ (vide supra). Based on the idea that relaxation of $^1P^*B_AH_AQ_A$ state precedes the primary charge separation (see Eq. (10)) the value of -0.07 eV appears to be most realistic for ΔG_{12} in control suspensions of RCs.

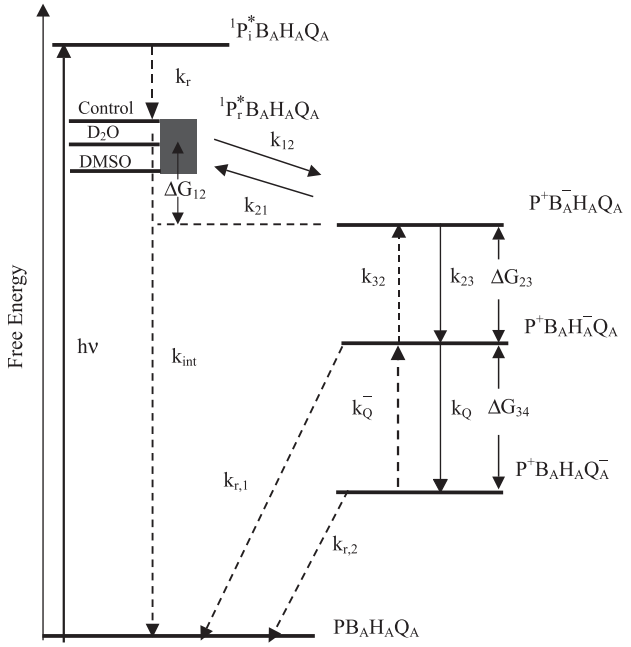

Fig. 5. Energetic scheme of the charge separation and electron transfer reactions in the RC of *Rb. sphaeroides* purple bacterium. $^1P_i^*B_AH_AQ_A$ and $^1P_r^*B_AH_AQ_A$ are the initial and relaxed excited states of the primary electron donor; k_r denotes the relaxation rate constant of $^1P_i^*B_AH_AQ_A$ energy level; B_A^- and H_A^- are the anion radical of BChl and BPheo molecules, respectively; k_{12} and k_{23} are the rate constants of the direct electron transfer; k_{21} and k_{32} are the rate constants of the back electron transfer; k_Q and k_Q^- are the rate constants of the direct ($H_A^- \rightarrow Q_A$) and back ($H_A \leftarrow Q_A^-$) electron transfer reactions, respectively; k_{r1} and k_{r2} are recombination rate constants; k_{int} is the intramolecular deactivation rate constant; ΔG_{12} is the free energy gap between $^1P_r^*B_AH_AQ_A$ and $P^+B_A^-H_AQ_A$ energetic levels; ΔG_{23} and ΔG_{34} are the free energy gaps between the corresponding levels of states $P^+B_A^-H_AQ_A$, $P^+B_AH_A^-Q_A$ and $P^+B_AH_AQ_A^-$. Distinction in the free energy gaps ΔG_{12} for control, D_2O and DMSO treated RC samples is indicated by the grey box.

After D_2O/H_2O exchange, the energy change due to D-bond deformation will be at least $\sqrt{2}$ times larger than in the case of H-bonds. As a consequence, the $^1P_r^*B_AH_AQ_A$ (D) state preceding the electron transfer in the samples modified by D_2O/H_2O exchange should be lower in energy than the $^1P_r^*B_AH_AQ_A$ (H) state formed in the control samples. Thus, the ratio of rate constants k_e' and $(k_e')^-$ are expected to become changed and the charge separation time increased as is observed in our experiments. The band shift of the fluorescence spectra shown in Fig. 2 supports this conclusion. Since hydrogen bond deformation(s) as a response to $^1P_i^*B_AH_AQ_A$ state formation is (are) much faster than fluorescence emission, the latter originates from $^1P_r^*B_AH_AQ_A$ state and the shift of the fluorescence spectra to longer wavelengths is a measure of the energy change owing to $^1P_i^*B_AH_AQ_A$ state solvation in different sample types. In the case of modification by D_2O/H_2O exchange, this solvation energy is larger by about 0.011 eV than in control samples (see Table 1). As a consequence, a value of $\Delta G_{12} = -0.059$ eV should be used in Eq. (5) for calculation of the rate constant k_{ET} of charge separation in D_2O-treated RC.

Glycerol and DMSO differ in their modifying effects on the structure of proteins and the state of hydrogen bonds in RC. It is known [47,48] that glycerol affects the hydration layer of proteins and decreases the amplitude of thermal motion of the polypeptide chain. Moreover, this solvent is characterized by extremely high viscosity and low capacity to penetrate into the protein structure. This specific manner of interaction with proteins is assumed to be responsible for a glycerol-induced shift of the midpoint potential of cofactors without significant distortion of the hydrogen bond network in the nearest environment. As a result, addition of 70% (v/v) glycerol has virtually no effects on τ_e and τ_Q, see Table 2. On the other hand, DMSO is characterized by high proton-acceptor capacity [32,49] and the capability to penetrate into the hydrophobic part of the RC [41,50]. This solvent is able to displace free water from biological structures leading to a diminished amount of bound water and the incorporation of DMSO into the hydrogen bond network of macromolecules [41,49]. It was demonstrated in Refs. [32,33] that the addition of DMSO to H-bonded liquids causes an increase in the rigidity of the hydrogen bonds. Furthermore, DMSO changes the dielectric constant ε of the medium. Accordingly, one can expect that, in DMSO-treated samples, the solvation energy of the ^1P_i* state will be larger than in control samples. This idea is in perfect qualitative agreement with the data in Fig. 2. The fluorescence spectra of RCs modified by 35% (v/v) DMSO are shifted to the red by 14.5 nm (see Table 1). This spectral shift corresponds to the lowering of the $^1P_r^*$ level by ~ 0.022 eV in comparison to the position of the $^1P_r^*$ level in control samples. Therefore a value of -0.048 eV should be used for ΔG_{12} in RCs suspended in suspension containing DMSO. As a result, the rate constant of charge separation in the DMSO-modified RCs decreases in comparison with the $k_e = 1/\tau_e$ value in control as well as in D_2O/H_2O substituted samples (see Table 2). Thus, modifications of the reaction center hydrogen bond network by means of $D_2O \rightarrow H_2O$ exchange or by DMSO addition leads to changes of parameters ΔG and λ and, consequently, of the value of k_{ET} (Eq. (5)).

An analytical description of the charge separation process and the electron transfer to quinone Q_A in normal and modified RC preparations will now be presented within the framework of an energy scheme of the electron transfer reactions that is depicted in Fig. 5. This energetic scheme is based on the following assumptions and experimental data, mentioned above:

(a) in the RCs charge separation starts from the relaxed state $^1P_r^*B_AH_AQ_A$;
(b) the monomeric bacteriochlorophyll molecule B_A serves as primary electron acceptor. The free energy gap ΔG_{12} ($^1P_r^*B_AH_AQ_A - P^+B_A^-H_AQ_A$) for control samples, D_2O- and DMSO-treated RC preparations (see Fig. 5) was chosen to be of -0.07, -0.059 and -0.048 eV, respectively;
(c) ultrafast electron transfer from B_A^- to H_A generates the initial state $\{P^+B_AH_A^-Q_A\}_i$. The free energy difference ΔG ($P^+B_A^-H_AQ_A - \{P^+B_AH_A^-Q_A\}_i$) was taken to be about -0.14 eV according to Ref. [36] as well as to the results obtained in this paper (see below);
(d) the subsequent electron transfer from H_A^- to Q_A takes place with a reaction time of 200 ps in control samples, $\sim$ 350 ps in the RCs treated by D_2O/H_2O exchange and within 510 ps in samples modified by 35% (v/v) DMSO addition;
(e) a value of 0.9 ps^{-1} is used for k_{23} in accordance with data published in Refs. [12,13].

For the sake of simplicity, the back reactions $P^+B_AH_A^-Q_A \xrightarrow{k_{32}} P^+B_A^-H_AQ_A$ and $P^+B_AH_AQ_A^- \xrightarrow{k_Q^-} P^+B_AH_A^-Q_A$ were ignored. Under these conditions, the solution of the set of kinetic equations for the time dependent population $P_1(t)$, $P_2(t)$ and $P_3(t)$ of the energy levels $^1P_r^*B_AH_AQ_A$, $P^+B_A^-H_AQ_A$ and $P^+B_AH_A^-Q_A$, respectively, participating in electron transfer reactions can be written as:

$$P_1(t) = a_1\exp(-t/\tau_1) + a_2\exp(-t/\tau_2)$$

$$P_2(t) = b_1\exp(-t/\tau_1) + b_2\exp(-t/\tau_2) \quad (11)$$

$$P_3(t) = c_1\exp(-t/\tau_1) + c_2\exp(-t/\tau_2) + c_3\exp(-t/\tau_3)$$

where:
$a_1 = (\lambda_1 - k_{21} - k_{23})/(\lambda_1 - \lambda_2)$; $a_2 = (k_{21} + k_{23} - \lambda_2)/(\lambda_1 - \lambda_2)$; $b_1 = k_{12}/(\lambda_1 - \lambda_2)$; $b_2 = -b_1$; $c_1 = k_{12}k_{23}/((\lambda_1 - \lambda_2)(\lambda_1 - k_3))$; $c_2 = -k_{12}k_{23}/((\lambda_1 - \lambda_2)(\lambda_2 - k_3))$; $c_3 = k_{12}k_{23}/((\lambda_1 - k_3)(\lambda_2 - k_3))$; $\lambda_1 = (k_{12} + k_{21} + k_{23})/2 + 1/2((k_{12} + k_{21} + k_{23})^2 - 4k_{12}k_{23})^{1/2}$; $\lambda_2 = (k_{12} + k_{21} + k_{23})/2 - 1/2((k_{12} + k_{21} + k_{23})^2 - 4k_{12}k_{23})^{1/2}$; $\tau_1 = 1/\lambda_1$; $\tau_2 = 1/\lambda_2$; $k_3 = k_Q$.

The relationship between the rate constant of forward (k_e) and back (k_e^-) electron transfer reactions is described by:

$$k_e^- = k_e\exp(-|\Delta G|/k_BT) \quad (12)$$

In the calculations, we varied the value of the forward electron transfer rate k_{12}, while the value of k_{21} was determined according to Eq. (12).

Time courses of the populations $P_1(t)$, $P_2(t)$ and $P_3(t)$ are shown in Fig. 6. It should be noted that experimentally the rate constants $k_e = 1/\tau_e$ and $k_Q = 1/\tau_Q$, Table 2, were gathered from the light-induced absorption changes ΔA665. The ΔA665 change corresponds to the time course of curve $P_3(t)$ in Fig. 6. There is a great number of mutually correlated families of $P_1(t)$, $P_2(t)$ and $P_3(t)$ curves. Fig. 6 presents only that curves where the time course of P_3 coincides with the experimentally recorded kinetics of the DA665 change in control samples (Fig. 6a) and samples modified either by D_2O/H_2O substitution (Fig. 6b) or by DMSO addition (Fig. 6c). The remaining parameters used in Eq. (11) for calculating $P_1(t)$, $P_2(t)$ and $P_3(t)$ are taken from Table 4.

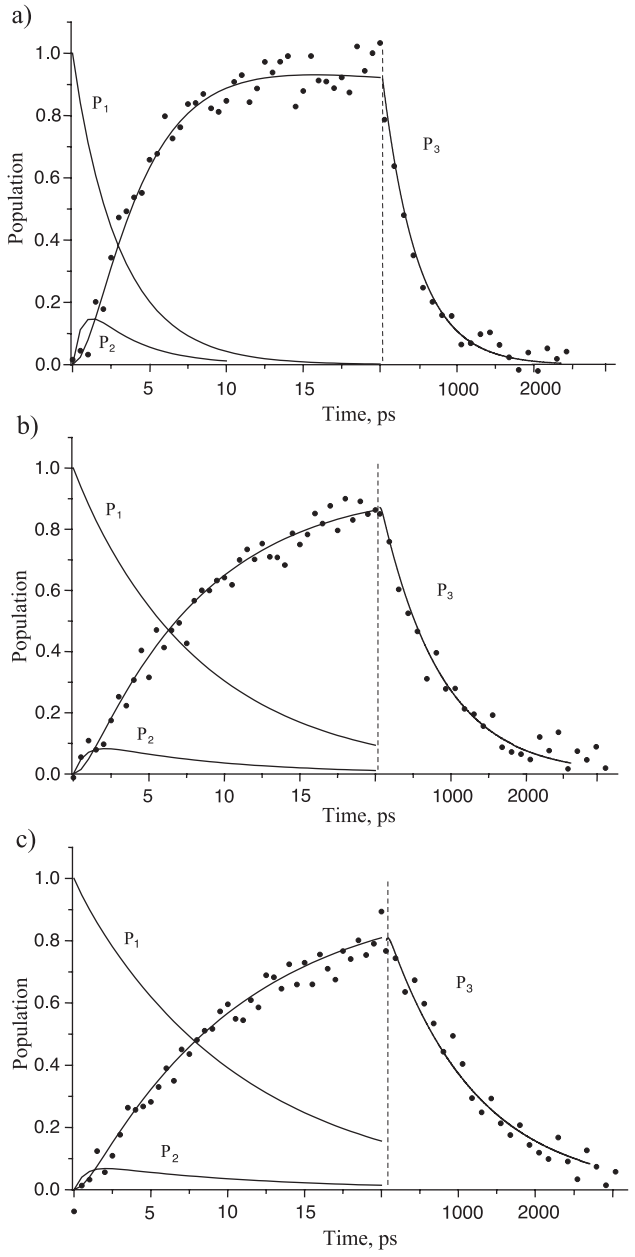

Fig. 6. Time dependence of populations of the $^1P_r^*B_AH_AQ_A$ (P_1), $P^+B_A^-H_AQ_A$ (P_2) and $P^+B_AH_A^-Q_A$ (P_3) states calculated according to Eq. (11). (a) Model curves P_1, P_2 and P_3 calculated at the following values of parameters: $\Delta G_{12} = -70$ meV; k_{12}=(3.3 ps)$^{-1}$; k_{21}=(54 ps)$^{-1}$; k_3=(200 ps)$^{-1}$. ●—Experimentally measured kinetics of ΔA665 light-induced absorption changes in control samples of RC. (b) $\Delta G_{12} = -59$ meV; k_{12}=(8.4 ps)$^{-1}$; k_{21}=(89 ps)$^{-1}$; k_3=(350 ps)$^{-1}$. ●—Experimentally measured kinetics of ΔA665 light-induced absorption changes in the RC samples modified by D_2O/H_2O substitution. (c) $\Delta G_{12} = -48$ meV; k_{12}=(10.65 ps)$^{-1}$; k_{21}=(73 ps)$^{-1}$; k_3=(510 ps)$^{-1}$. ●—Experimentally measured kinetics of ΔA665 light-induced absorption changes in the RC samples modified by DMSO (35% v/v) addition. The value k_{23}=(0.9 ps)$^{-1}$ was used for the calculation of all curves. The values of the other parameters in Eq. (11) are shown in Table 4. Experimental kinetic P_3 was obtained using the real kinetic of ΔA665 absorption changes deconvoluted with apparatus function of the registration system and reduced to the population of $P^+B_AH_A^-Q_A$ state.

In the following, the implications of the fit of the time courses in Fig. 6 will be discussed.

4.4. Linear electron transport leading to $P^+B_AH_AQ_A^-$ formation

In control RC samples the experimentally determined time constants τ_e and τ_Q are ~ 3.4 and 205 ps, respectively (see Table 2). According to the energetic scheme of light-induced reactions in bacterial reaction centers, the decay of the $P^+B_AH_A^-Q_A$ state occurs due to electron transfer to the quinone acceptor Q_A only. For this reason, the value of k_3, Eq. (11), was taken to be $k_3 = k_Q = 1/\tau_Q$. The time of electron transfer from B_A^- to H_A ($1/k_e''$ in Eq. (10)) was taken to be 0.9 ps according to values reported in [12,13]. With these values, a good agreement of the experimental time course of ΔA665 with the calculated curves $P_3(t)$ could be obtained with the following parameter values: $\Delta G_{12} = -0.07$ eV, $k_e' = k_{12} = 3.0 \times 10^{11}$ s^{-1} (τ_{12}=3.3 ps) and $(k_e'')^- = k_{21} = k_{12}\exp(-\Delta G_{12}/kT) = 1.85 \times 10^{10}$ s^{-1} (τ_{21}=54 ps). As can be seen from Table 4, the use of these values to fit the experimental data for control RC preparations leads to practically monoexponential kinetics for decay and formation of states $^1P_r^*B_AH_AQ_A$ ($P_1(t)$ in Fig. 6a) and $P^+B_AH_A^-Q_A$ ($P_3(t)$ in Fig. 6a), respectively, with τ_2 = 3.4 ps. The value of τ_2 (Table 4) coincides with that of τ_e (Table 2). The analysis also reveals that the transient population of state $P^+B_A^-H_AQ_A$ ($P_2(t)$ in Fig. 6a) contributes only to a small extent to the transient absorption kinetics. Furthermore, Fig. 6a reveals that $P^+B_A^-H_AQ_A$ population reaches its maximum value of 0.16 at a time t = 1.6 ps after the excitation of P.

In D_2O-modified RC preparations, the time constants τ_e and τ_Q determined via flash-induced absorption changes ΔA665(t) are ~ 8.5 and ~ 350 ps (see Table 2). From a comparison of the fluorescence spectra of control and D_2O-modified RCs (Fig. 2, Table 1) and the theoretical calculations reported in this paper (see above), the value of ΔG_{12} (see Fig. 5) was taken to be −0.059 eV. The time of electron transfer from B_A^- to H_A is $\tau_{23} = 1/k_{23} = 0.9$ ps [12,13]. In this case, a good agreement between the experimental kinetics of ΔA665 in D_2O-modified RCs and the calculated curve ($P_3(t)$ in Fig. 6b) is obtained for $k_{12} = 1.19 \times 10^{11}$ s^{-1} (τ_{12}=8.4 ps) and $k_{21} = 1.12 \times 10^{10}$ s^{-1} (τ_{21}=89 ps). An inspection of Fig. 6b and the data of Table 4 reveal that, in RCs suspended in D_2O buffer, the kinetics of electron transfer from $^1P_r^*$ (curve $P_1(t)$) and of $P^+B_AH_A^-Q_A$ formation (rise time of $P_3(t)$) are close to monoexponential curves with τ_2 = 8.5 ps, coinciding with the charge separation time τ_e found experimentally (Table 2). In these samples, the calculated maximum population of the transient state $P^+B_A^-H_AQ_A$ (curve $P_2(t)$ in Fig. 6b) of 0.081 at t = 2.24 ps is markedly smaller than in the control.

In DMSO-modified RC preparations, τ_e and τ_Q are ~ 10.8 and 510 ps, respectively (Table 2). From a comparison of the fluorescence spectra of control and DMSO-modified RCs (Fig. 2) and the theoretical calculations

Table 4
Parameters of Eq. (11) used for calculating theoretical curves $P_i(t)$ ($i=1,2,3$) shown in Fig. 6

Sample	Parameters of approximation										
	a_1	a_2	b_1	b_2	c_1	c_2	c_3	τ_1, ps	τ_2, ps	τ_3, ps	ΔG_{12}, meV
Control	0.008	0.992	−0.36	0.36	−1.38	0.36	1.02	0.88	3.4	200	−70
D_2O/H_2O exchange	0.001	0.999	−0.12	0.12	−1.15	0.12	1.03	0.89	8.5	350	−59
35% DMSO addition	0.001	0.999	−0.091	0.091	−1.11	0.09	1.02	0.89	10.8	510	−48

$a_{1,2}$, $b_{1,2}$, $c_{1,2,3}$ are the coefficients; τ_1, τ_2, τ_3 are time constants; ΔG_{12} is the free energy gap between energy levels of $^1P_r^*B_AH_AQ_A$ and $P^+B_A^-H_AQ_A$ states, Fig. 5.

reported in this paper (see above), the value of ΔG_{12} (see Fig. 5) was taken to be −0.048 eV. When using $\tau_{23}=0.9$ ps and $\Delta G_{12}=-0.048$ eV, a good fit of the experimental ΔA665 kinetics by the theoretical curve ($P_3(t)$ in Fig. 6c) was obtained with $k_{12}=9.4\times10^{10}$ s^{-1} ($\tau_{12}=10.65$ ps), $k_{21}=1.37\times10^{10}$ s^{-1} ($\tau_{21}=73$ ps). Other parameters used for the fit of the experimental data are compiled in the lower part of Table 4.

The kinetics of charge separation and $P^+B_AH_A^-Q_A$ formation in these samples show a nearly monoexponential time course with $\tau_2=10.8$ ps. This value of the time constant coincides with that one measured for τ_e in DMSO-treated RCs (see Table 2).

4.5. Charge recombination $P^+B_AH_A^-\rightarrow PB_AH_A$

In RCs where the electron transfer from H_A^- to Q_A is blocked, either by reducing Q_A in the dark or by extracting the electron acceptor Q_A, the lifetime of the radical pair $P^+B_AH_A^-$ was found to be 11–13 ns [26,35,36]. In this section, the symbol Q_A is omitted to illustrate that this component is nonfunctional.

At room temperature, the kinetics of this recombination reaction between P^+ and H_A^- is nearly monoexponential with $\tau_2=11.2$ ns [26]. On the other hand, it was shown in Refs. [35,46] that the decay kinetics of $^1P^*$ comprise fast components (~ 0.6 and 3.5 ns) that are related to the recombination reaction patterns. Obviously, the "averaged" recombination time measured in our experiments has to be shorter than the slowest (~ 13 ns) recombination decay component observed in Refs. [35,36,46].

The ratio of the rate constants for the forward ($^1P_r^*B_AH_A\rightarrow P^+B_AH_A^-$) and the corresponding back reaction, i.e. $(k_e=3.5\text{ ps})^{-1}/k_e^-=(11.2\text{ ns})^{-1}$ corresponds with a difference of the apparent free energy ΔG ($^1P_r^*B_AH_A-(P^+B_AH_A^-)$) of $\Delta G=-0.2$ eV.

In marked contrast to samples with nonfunctional Q_A suspended in control buffer the decay of flash-induced ΔA665 nm absorption changes clearly deviates from a monoexponential decay kinetics in modified suspensions. Analytically, the experimental kinetics of the photoinduced changes of ΔA665 were fitted with Eq. (4) after convolution with the apparatus function of the spectrometer [26]. The amplitude A_3 of the third component in Eq. (4) for the ΔA665 fit was taken to be zero. It was found in Ref. [26] that, in RC preparations where exchangeable protons are replaced by deuterons, a new fast component with $\tau_1=0.5$ ns and a normalized amplitude of $A_1=0.35$ appears in addition to the slow component with $\tau_2=11$ ns and $A_2=0.65$. The value of $\tau_2=11$ ns corresponds with that of the nearly monoexponential kinetics in control samples. In the RCs modified by DMSO addition, the kinetics of the ΔA665 decay was also biexponential with a fast ($\tau_1=0.8$ ns, $A_1=0.52$) and a slow ($\tau_2=10.8$ ns, $A_2=0.48$) components.

The states $^1P_r^*B_AH_A$ and $(P^+B_AH_A^-)_i$ formed immediately after excitation and charge separation, respectively, are nonequilibrium states (vide supra). The response of the water–protein surroundings to the generation of nonequilibrium states of cofactors causes subsequent microconformational reorganization of the medium followed by a solvation process. Solvation is a continuous process with a distinct temporal hierarchy. The fastest response of the medium is the equilibration of the $^1P_r^*B_AH_A$ state due to deformation of hydrogen bonds. The $(P^+B_AH_A^-)_i$ state is also substantially out of equilibrium [36]. When the electron transfer to Q_A is blocked the lifetime of the $P^+B_AH_A^-$ state is 11–13 ns in control samples (vide supra). Obviously, the solvation processes are proceeding in this time domain. As a result, the energy level of the ion-radical pair $P^+B_AH_A^-$ decays from the initial state $(P^+B_AH_A^-)_i$ to the relaxed state $(P^+B_AH_A^-)_r$ faster than the recombination takes place.

We conclude that in the control samples the relaxation process of $(P^+B_AH_A^-)_i$ is fast and (taking into consideration the accuracy of the measurement) the kinetics of recombination can be considered as monoexponential with $\tau_2=11.2$ ns. In suspensions modified by D_2O/H_2O substitution, the extrapolation to the fast component ($\tau_1=0.5$ ns) yields an apparent free energy gap between states $(P^+B_AH_A^-)_i$ and $(P^+B_A^-H_A)$, ΔG_i $((P^+B_AH_A^-)_i-(P^+B_A^-H_A))\cong-0.13$ eV, whereas the apparent free energy gap of the relaxed state ΔG_r $((P^+B_AH_A^-)_r-(P^+B_A^-H_A))$ at $\tau_2=11.2$ ns is about −0.2 eV. The real kinetics of the recombination reaction represents a continuous distribution of life times from the fast (ΔG_i) down to the slow (ΔG_r) time range.

5. Concluding remarks

In the present study, the effects of protein relaxation on the kinetics and energetics of light-induced charge separation in anoxygenic purple bacteria have been analyzed

with special emphasis on the role of deformation of hydrogen bonds. It is shown that reorientation of hydrogen bonds provides the major contribution to the very fast environmental response to electronic excitation of the special pair and subsequent primary electron transfer steps. Based on simplified model calculations, the energy change owing to a proton shift within a hydrogen bond is estimated to be of the order 1–2 meV. This short-range relaxation of the protein matrix in the nearest environment of the cofactors upon their turnover is assumed to be of key relevance for achieving a very efficient charge separation taking place with a quantum yield of 100% [30]. Different effects are induced by replacement of exchangeable protons by deuterons and the addition of either DMSO or glycerol. In the former case, only the kinetics of electron transfer steps are retarded while in the presence of 70% glycerol only the midpoint potential of P/P^+ is shifted by 30 mV towards higher values. On the other hand, DMSO affects both the kinetics and the energetics.

Rate constants k_{ET} of nonadiabatic electron transfer steps can be regulated via modification of V_{ET}, ΔG^0 or λ. The present study shows that the change in the Gibbs standard free energy ΔG^0 originating from solvation of the nonequilibrium state $^1P^*$ can be regarded as the medium reorganization energy λ. Modifications induced by D_2O/H_2O exchange or DMSO addition can also change the quantum mechanical coupling element V_{ET} due to the alteration of the distances between cofactors, their orientation and of the energy of intermolecular interaction (dielectric constant ε, dipole moments). It was shown earlier [39] that the dielectric constant exerts a minor influence on the electron transfer rate constant: the ratio $k_{ET}(\varepsilon_1)/k_{ET}(\varepsilon_2) = 0.96$ for $\varepsilon_1 = 2\varepsilon_2$. One can expect that intermolecular distances and mutual orientation of their dipole moments will change owing to penetration of solvent molecules into the protein globule. This phenomenon is a subject of further investigations.

Acknowledgements

We are very grateful to Prof. J. Voigt for the many stimulating discussions and to Dr. D. Leupold for the assistance in measuring the fluorescence spectra.

This work was supported by the Russian Foundation for Basic Research, project no. 01-04-48254 and 01-04-48482, Universities of Russia, project UR.07.03.012, INTAS, project 00281 and by the International Bureau of BMBF, Germany, project RUS 00/204.

References

[1] C.R.D. Lancaster, U. Ermler, H. Michel, The structure of photosynthetic reaction centers from purple bacteria as revealed by X-ray crystallography, in: R.E. Blankenship, M.T. Madigan, C.E. Bauer (Eds.), Anoxygenic Photosynthetic Bacteria, Kluwer Academic Publishers, Netherlands, 1995, pp. 503–526.

[2] G.R. Fleming, R. Van Grondelle, The primary steps of photosynthesis, Phys. Today 47 (1994) 48–55.

[3] O. El-Kabbani, C.H. Chang, D.M. Tiede, J.R. Norris, M. Shiffer, Comparison of reaction centers from *Rhodobacter sphaeroides* and *Rhodopseudomonas viridis*: overall architecture and protein–pigment interactions, Biochemistry 30 (1991) 5361–5369.

[4] U. Ermler, G. Fritsch, S.K. Buchanan, H. Michel, Structure of the photosynthetic reaction centre from *Rhodobacter sphaeroides* at 2.65 Å resolution: cofactors and protein–cofactors interactions, Structure 2 (1994) 925–936.

[5] J. Deisenhofer, H. Michel, Crystallographic refinement at 2.3 Å resolution and refined model of the photosynthetic reaction center of *Rhodopseudomonas viridis*, J. Mol. Biol. 246 (1995) 429–457.

[6] E. Katilius, Z. Kataliene, S. Lin, A.K.W. Taguchi, N.W. Woodbury, B side electron transfer in a *Rhodobacter sphaeroides* reaction center mutant in which the B side monomer bacteriochlorophyll is replaced with bacteriopheophytin: low-temperature study and energetics of charge-separated states, J. Phys. Chem. B 106 (2002) 1471–1475.

[7] A.L. de Boer, S. Neerken, R. de Wijn, H.P. Permentier, P. Gast, E. Vijgenboom, A.J. Hoff, High yield of B-branch electron transfer in a quadruple reaction center mutant of the photosynthetic bacterium *Rhodobacter sphaeroides*, Biochemistry 41 (2002) 3081–3088.

[8] C. Kirmaier, P.D. Laible, D.K. Hanson, D. Holten, B-side charge separation in bacterial photosynthetic reaction centers: nanosecond time scale electron transfer from H_B^- to Q_B, Biochemistry 42 (2003) 2016–2024.

[9] M.C. Wakeham, M.G. Goodwin, C. McKibbin, M.R. Jones, Photoaccumulation of the $P^+Q_B^-$ radical pair state in purple bacterial reaction centres that lack the Q_A ubiquinone, FEBS Lett. 540 (2003) 234–240.

[10] C. Kirmaier, D. Holten, W.W. Parson, Temperature and detection-wavelength dependence of the picosecond electron-transfer kinetics measured in *Rhodobacter sphaeroides* reaction centers. Resolution of new spectral kinetic components in the primary charge-separation process, Biochim. Biophys. Acta 810 (1985) 33–48.

[11] V.A. Shuvalov, L.N.M. Dyusens, Primary electron transfer reactions in modified reaction centers from *Rhodopseudomonas sphaeroides*, Proc. Natl. Acad. Sci. U. S. A. 83 (1986) 1690–1694.

[12] W. Holzapfel, U. Finkele, W. Kaiser, D. Osterhelt, H. Scheer, H.U. Stilz, W. Zinth, Observation of a bacteriochlorophyll anion radical during the primary charge separation in a reaction center, Chem. Phys. Lett. 160 (1989) 1–7.

[13] A.R. Holzwarth, M.G. Muller, Energetics and kinetics of radical pairs in reaction centers from *Rhodobacter sphaeroides*. A femtosecond transient absorption study, Biochemistry 35 (1996) 11820–11831.

[14] N. Ivashin, S. Larsson, Vibrational mechanism for primary charge separation in the reaction center of *Rhodobacter sphaeroides*, J. Phys. Chem. B 106 (2002) 3996–4009.

[15] H. Xu, R.-B. Zhang, S.-H. Ma, Z.-W. Qu, X.-K. Zhang, Q.-Y. Zhang, Theoretical studies on the mechanism of primary electron transfer in the photosynthetic reaction center of *Rhodobacter sphaeroides*, Photosynth. Res. 74 (2002) 11–36.

[16] H.-W. Trissl, K. Bernhardt, M. Lapin, Evidence for protein dielectric relaxations in reaction centers associated with the primary charge separation detected from *Rhodospirillum rubrum* chromatophores by combined photovoltage and absorption measurements in the 1–15 ns time range, Biochemistry 40 (2001) 5290–5298.

[17] F. van Mourik, M. Rens, A.R. Holzwarth, Long-lived charge-separated states in bacterial reaction centers isolated from *Rhodobacter sphaeroides*, Biochim. Biophys. Acta 1504 (2001) 311–318.

[18] J.C. Williams, R.G. Alden, M.A. Murchison, J.M. Peloquin, N.W. Woodbury, J.P. Allen, Effect of mutation near the bacteriophyll in the reaction centers from *Rhodobacter sphaeroides*, Biochemistry 31 (1992) 11029–11037.

[19] M.A. Murchison, R.G. Alden, J.P. Allen, J.M. Peloquin, A.K.W. Taguchi, N.W. Woodbury, J.C. Williams, Mutations designed to modify the environment of the primary electron donor of the reaction

center from *Rhodobacter sphaeroides*: phenylalanine to leucine at L167 and histidine to phenylalanine at L168, Biochemistry 32 (1993) 3498–3505.
[20] T.A. Mattioli, J.C. Williams, J.P. Allen, B. Robert, Changes in primary donor hydrogen-bonding interactions in mutant reaction centers from *Rhodobacter sphaeroides*: identification of the vibrational frequencies of all the conjugated carbonyl groups, Biochemistry 33 (1994) 1636–1943.
[21] X. Lin, H.A. Murchison, V. Nagarajan, W.W. Parson, C.J. Williams, J.P. Allen, Specific alteration of the oxidation potential of the electron donor in the reaction centers from *Rhodobacter sphaeroides*, Proc. Natl. Acad. Sci. U. S. A. 91 (1994) 10265–10269.
[22] T.A. Mattioli, X. Lin, J.P. Allen, J.C. Williams, Correlation between multiple hydrogen oxidation potential of the bacteriochlorophyll dimer of reaction center from *Rhodobacter sphaeroides*, Biochemistry 34 (1995) 6142–6152.
[23] A. Ivancich, K. Arltz, J.C. Williams, J.P. Allen, T.A. Mattioli, Effects of hydrogen bonds on the redox potential and electronic structure of the bacterial primary electron donor, Biochemistry 37 (1998) 11812–11820.
[24] E.J. Bylina, C. Kirmaier, L. McDowell, D. Holten, D.C. Youvan, Influence of an amino-acid residue on the optical properties and electron transfer dynamics of a photosynthetic reaction centre complex, Nature 336 (1988) 182–184.
[25] V.Z. Paschenko, B.N. Korvatovsky, S.L. Logunov, P.P. Knox, N.I. Zakharova, N.P. Grishanova, A.B. Rubin, Modification of protein hydrogen bonds influences the efficiency of picosecond electron transfer in bacterial reaction centers, FEBS Lett. 214 (1987) 28–34.
[26] V.Z. Paschenko, V.V. Gorokhov, N.P. Grishanova, E.A. Goryacheva, B.N. Korvatovsky, P.P. Knox, N.I. Zakharova, A.B. Rubin, The influence of structural-dynamic organization of RC from purple bacterium *Rhodobacter sphaeroides* on picosecond stages of photoinduced reactions, Biochim. Biophys. Acta 1364 (1998) 361–372.
[27] V.Z. Paschenko, P.P. Knox, S.K. Chamorovsky, P.M. Krasilnikov, M.D. Mamedov, A.Yu. Semenov, N.I. Zakharova, G. Renger, A.B. Rubin, Effect of D_2O and cryosolvents on the redox properties of bacteriochlorophyll dimer and electron transfer processes in *Rhodobacter sphaeroides* reaction centers, Bioelectrochemistry 53 (2001) 233–241.
[28] V.Z. Paschenko, Correlation between structural-dynamic organization of the reaction centers of the purple bacterium *Rhodobacter sphaeroides* and the picosecond stages of photosynthesis, Biophysics 45 (2000) 449–456.
[29] N.I. Zakharova, I.Yu. Churbanova, Methods of reaction center preparations from photosynthetic purple bacteria, Biochemistry 65 (2000) 181–193.
[30] C.A. Wright, R.K. Clayton, The absolute quantum efficiency of bacteriochlorophyll photooxidation in reaction centres of *Rhodopseudomonas sphaeroides*, Biochim. Biophys. Acta 333 (1973) 246–260.
[31] V.S. Chirvony, V.A. Galevsky, N.N. Kruk, B.M. Dzagarov, P.-Y. Turpin, Photophysics of cationic 5,10,15,20-tetrakis-(4-*N*-methylpyridyl)porphyrin bound to DNA, $[poly(dA\text{-}dT)]_2$ and $[poly(dG\text{-}dC)]_2$; on a possible charge transfer process between guanine and porphyrin in its excited singlet state, J. Photochem. Photobiol. 40 (1997) 154–162.
[32] W.A.P. Luck, Role of hydrogen bonding in the structure of liquids, Acta Chim. Hung. 121 (1986) 119–145.
[33] H. Kleeberg, Influence of alkali cations on the infrared spectra of water molecules in aprotic solvents, J. Phys. Chem. 90 (1986) 4427–4430.
[34] S.K. Chamorovsky, M.D. Mamedov, A.Yu. Semenov, N.I. Zakharova, P.P. Knox, A.B. Rubin, The influence of glycerol and dimethylsulfoxide on the midpoint potential of bacteriochlorophyll dimer in *Rhodobacter sphaeroides* reaction center, Doklady Biochem. Biophys. (Moscow) 361 (1998) 120–122.
[35] G. Hartwich, H. Lossau, M.E. Michel-Beyerle, A. Ogrodnik, Nonexponential fluorescence decay in reaction centers of *Rhodobacter sphaeroides* reflecting dispersive charge separation up to 1 ns, J. Phys. Chem. B 102 (1998) 3815–3820.
[36] A. Ogrodnik, G. Hartwich, H. Lossau, M.E. Michel-Beyerle, Dispersive charge separation and conformational cooling of $P^+H_A^-$ in reaction centers of *Rb. sphaeroides* R26: a spontaneous emission study, Chem. Phys. 244 (1999) 461–478.
[37] R.A. Marcus, N. Sutin, Electron transport in chemistry and biology, Biochim. Biophys. Acta 811 (1985) 265–322.
[38] C.C. Moser, C.C. Page, X. Chen, P.L. Dutton, Intraprotein electron transfer: illustrations from the photosynthetic reaction center, in: G. Peschek, W. Loffelhandt, G. Schemetter (Eds.), The Phototropic Procaryotes, Plenum, New York, 1999, pp. 105–111.
[39] P.M. Krasil'nikov, V.V. Gorokhov, E.A. Goryacheva, P.P. Knox, V.Z. Paschenko, A.B. Rubin, Investigation of the electron transfer reactions and redox midpoint potential of photoactive bacteriochlorophyll in the reaction centers of *Rhodobacter sphaeroides* modified by D_2O and cryoprotectants, Biomembranes (Moscow) 17 (2000) 271–281.
[40] W. Brown, Dielectrics, in: S. Flugge (Ed.), Handbuch der Physik, vol. XVII, Springer, Berlin, 1961.
[41] S.I. Aksenov, I.I. Gavrilova, M.G. Gangard, O.P. Revokatov, Investigation of dimethylsulfoxide interaction with protein macromolecules using method of spin echo NMR, Kryobiology (Moscow) 4 (1985) 31–33.
[42] C. Rishel, D. Spiedel, J.P. Ridge, J. Breton, J.C. Lambry, J.L. Martin, M.H. Vos, Low frequency vibrational modes in proteins: changes induced by point-mutations in the protein-cofactor matrix of bacterial reaction centers, Proc. Natl. Acad. Sci. U. S. A. 95 (1998) 12306–12311.
[43] G. Fritzsch, L. Kampmann, G. Kapaun, H. Michel, Water clusters in the reaction centre of *Rhodobacter sphaeroides*, Photosynth. Res. 55 (1998) 127–132.
[44] M. Karplus, J.M. McCammon, Dynamics of protein: elements and function, Ann. Rev. Biochem. 53 (1983) 263–300.
[45] A. Nitzan, Ultrafast relaxation in water, Nature 402 (1999) 472–475.
[46] M. Volk, G. Aumeier, T. Langenbacher, R. Feick, A. Ogrodnik, Energetics and mechanism of primary charge separation in bacterial photosynthesis. A comparative study on reaction centers of *Rhodobacter sphaeroides* and *Chloroflexus aurantiacus*, J. Phys. Chem. B. 102 (1998) 735–751.
[47] A. Priev, A. Almagor, S. Yedgar, G. Savish, Glycerol decreases the volume and compressibility of protein interior, Biochemistry 35 (1996) 2061–2066.
[48] V.I. Goldanskii, Y.F. Krupyanskii, Protein dynamics: hydration, temperature and solvent viscosity effects as revealed by Rayleigh scattering radiation, in: R.B. Gregory (Ed.), Protein–Solvent Interactions, Marcel Dekker, New York, 1995, pp. 289–326.
[49] Yu.N. Kukushkin, Dimethylsulfoxide—an important aprotic solvent. Soros Ed. Journal 7 (1997) 54–59.
[50] R. Santucci, E. Laurenti, F. Sinibaldi, R.P. Ferrari, Effect of dimethylsulfoxide on the structure and the functional properties of horseradish peroxidase as observed by spectroscopy and cyclic voltammetry, Biochim. Biophys. Acta 1596 (2002) 225–233.